Switched Discharge Device for Enhanced Energy Extraction from Li-Ion 18650

Vasile Surducan and Olivia-Ramona Bruj *

National Institute for Research, Development of Isotopic and Molecular Technologies,
400293 Cluj-Napoca, Romania
* Correspondence: olivia.bruj@itim-cj.ro; Tel.: +4-0264-584037

Abstract: All autonomous electrically powered devices require a continuous power supply from batteries. Increasing the discharge performance is the top priority in the Lithium-Ion (Li-Ion) battery field and pulsed discharge is proving numerous advantages. In this paper, the maximum efficiency of pulsed discharge method on a constant load while the cells are alternately switched with dead-time is thoroughly studied. Therefore, a novel Li-Ion charge/discharge and measurement device (SWD) using fast switching MOSFET was designed and fabricated. The device can alternately switch up to 8.3 kHz two Li-Ion 18650 batteries, generating continuous power to the programmable load and monitor the parameters that impact the capacity of the battery. An EIS (Electrochemical Impedance Spectroscopy) analysis is employed to evaluate the impedance and the behavior of the cells at frequencies up to 10 kHz. Experimental results reveal that a maximum discharge time is determined when two cells are switched at a frequency of 5.8 kHz. As a consequence, the total capacity of two switched batteries in a single discharge cycle is increased by 16.6%. Pulsed discharge efficiency is visible starting from 70% State of Charge (SOC) and is correlated with the rest time, reduced heat loss and inductance, respectively.

Keywords: lithium-ion cells; pulsed discharge; alternate switching; energy surplus; specific frequency

1. Introduction

Li-Ion 18650 cells are commonly used by various household consumers, electric vehicles (EV) and power-walls. On these, the Li-Ion cell is used in an integrated battery system (controlled by a battery management system- BMS) that store electrical energy. In such applications, the amount of energy which can be extracted during each discharge cycle is crucial, because it defines the backup time. During this time, the EV battery or the power-wall is able to supply an external load. Li-Ion cells have an accepted voltage swing between fully charged (4.2 V) and fully discharged (2.5 V) thresholds [1,2]. Exceeding these limits lowers the cell lifecycle and may irreversibly damage the cell. Jiang et al. [3] defined the maximum available energy as the amount of energy that can be released from a battery starting from a fully charged state during continuous discharge. In order to enhance the amount of energy extracted from a Li-Ion cell toward the maximum available energy, at least two methods can be used: (1) continuously discharging the cell under low current and (2) discharging the cell under pulsed current [4]. The first method limits the amount of instant power delivered by the cell and cannot be used in high power demand applications unless huge capacity cells (or parallel connected cells) are used. The second method is suitable for high power generation, but it requires additional hardware to extract the current pulses from the Li-ion cell with some well-defined parameters (frequency, duty-cycle, pulse shape, etc.). Such hardware should also be able to convert, with highest efficiency, the resulted pulsed voltage into continuous voltage required by the load. A review of the literature reveals several perspectives on Li-ion pulse discharge technique. For example, Benini et al. [5] switched alternately two Ni-MH packs at 50% duty cycle in 12 Hz–12 kHz

frequency range to supply a load at 3 A. It has been reported that discharge time can reach up to 200% compared with continuous discharge, although the source of the energy required for switching (the Ni-MH battery itself or an external power supply) was not disclosed, nor the energy loss on the diodes, which require to be connected in series with each battery pack, to avoid reversed current flow. Unfortunately, no discharge curve graphics or energy extracted values have been provided in the paper. Pulsed discharge methods have also been studied by DuBeshter and Jorne in [6] and Qin et al. in [7] and improved characteristics in terms of discharge time, temperature and capacity retention have been disclosed. Furthermore, in [8], Chen et al., studied the optimum discharging frequency (considered to be 1055 Hz) of a Li-Ion cell (4.2 V/1500 mAh) corresponding to the minimum AC impedance (0.0834 Ω) of the cell. Compared to continuous discharge and to other switching frequencies higher than optimum, only a 0.9% improvement has been obtained. Several theoretical energy estimating methods have been proposed in [9,10] for the continuous discharge, but energy calculations for pulsed discharge have not been investigated in the literature.

For this reason, our main focus is to determine the maximum efficiency in terms of capacity and energy extracted, in a single discharge cycle, when pulsed method in alternately switched mode is employed. In this context, the scope of this work was to design and manufacture a dedicated device (SWD) for the precise measurement of the power delivered to a constant load under pulsed or switched discharge. SWD is a programmable device with power MOSFET (metal-oxide-semiconductor-field-effect-transistor) switches, active load, voltage, current, time, temperature measurement and USB communication that can be used for switching frequencies up to 8.3 kHz. The condition for this approach to be efficient is for the energy consumed on the switching circuit to be as small as possible. Based on SWD generated data, the monitored parameters during experiment were: the optimum frequency discharge (f_{Zmin}), discharging time between voltage swing limits, delivered power, Li-Ion cell capacity and temperature. Aiming for the maximum energy output, and according to [8], our initial switched discharge started with the frequency corresponding to the minimum impedance. Thus, to obtain f_{Zmin}, AC impedance analysis has been performed in our laboratory using EIS technique. The variation of impedance spectrum at different SOC states via EIS method has been employed using a similar technique as presented in [11,12]. SOC is an indicator of the available capacity of a battery and well-defined experimental procedures has already been established in [8]. The most common way of SOC estimation is the Coulomb Counting method [13]. The EIS study and a Nyquist high frequency analysis are combined with switched discharge measurements to correlate the frequency impact on the capacity starting from 50% SOC level. Each type of measurement on SWD device was performed on three sets of two Panasonic NCR18650B cells, using more than 50 repetitions, for the reproducibility of the experiment. We plotted only one set of data to increase the intelligibility.

2. Materials and Methods

2.1. SOC and Impedance Measurement

SOC is the reference parameter that relates to the energy stored in a system and is quantified in terms of OCV. SOC measurements have been taken at room temperature (21 °C) over the entire interval with 10% resolution. The Coulomb Counting method has been used for SOC estimation because it gives a direct relationship with battery discharging current. The SOC measurements were preceded by capacity evaluation. Capacity measurement has followed the standard procedure: charging the batteries with CC-CV method and then discharged with 1C rate. After a full constant current-constant voltage (CC-CV) charge, a rest period of one hour followed. The limits for 100% SOC and 0% SOC were set to 4.15 V and 2.5 V, respectively. A 1C discharge current was set for the SOC characteristic with 30 min rest period between steps.

In order to find the minimum impedance and the corresponding frequency response of Li-Ion 18650 cells, EIS measurements have been performed on a VMP3B-5 module from the

VSP multi-channel potentiostat (BioLogic Science Instruments, Seyssinet-Pariset, France) controlled by EC-Lab software V11.46. Impedance measurements have been collected using the galvanostatic mode through Galvano Electrochemical Impedance Spectroscopy (GEIS) technique in EC-Lab software V11.46, where a small sinusoidal signal of 100 mA in the range 0.1 Hz to 10 kHz has been superimposed on a DC signal [14]. EIS data are measured through a Frequency Response Analyzer (FRA) based method, integrated within VSP.

2.2. Nyquist Plot Analysis

A Nyquist plot has been used to determine the frequency response at each SOC step. A simple Randle circuit for Li-Ion batteries includes a solution resistance R1 and two blocks of resistor-capacitor (RC) elements. Constant phase elements, Q3 and Q4, are preferred to account for non-ideal capacities and charge transfer resistances, R3 and R4, account for middle and low frequency spectrum [15,16]. The ohmic resistance is one of the main parameters used to characterize a battery and corresponds to the high-frequency intercept with the real axis [17]. In addition to that, the Randle equivalent circuit used to fit our EIS data are presented in Figure 1 and included an inductance, L2, parallel to the corresponding resistance parameter, R2, to account for the high frequency spectrum. The inductive behavior of a Li-ion cell is mostly associated with the measurement system components, such as current collectors and metallic contacts [18].
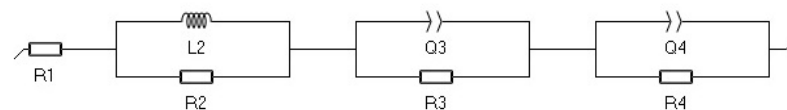
Figure 1. Nyquist equivalent circuit of Li-Ion cell used for data fitting in Ec-Lab.

2.3. SWD Device

An independent switching device (SWD), for continuous CC-CV charge and continuous, pulsed and pulsed switched discharge of one or two Li-Ion cells, has been designed and manufactured in our laboratory. Four frequencies were considered for measurements: 0.57 kHz, 2.3 kHz, 5.8 kHz and 8.3 kHz. The operating principle is presented in Figure 2.
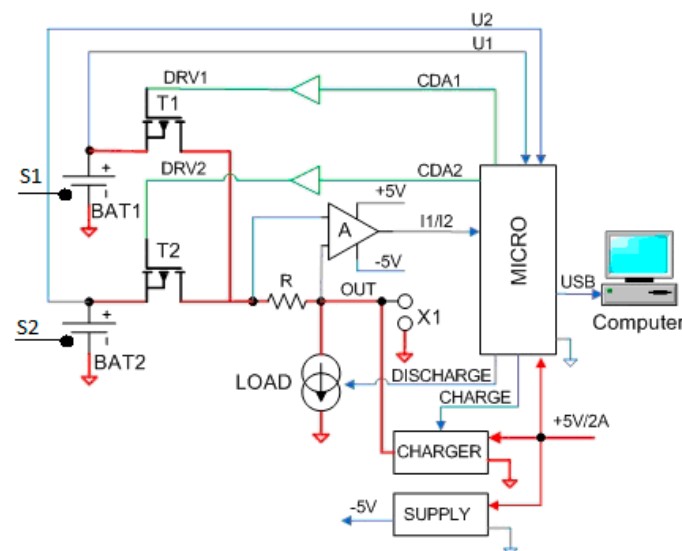
Figure 2. The SWD block schematic. BAT1, BAT2 = 18650 cells; S1, S2 = temperature sensors; T1, T2 = power switches, DRV1, DRV2 = gate drivers, R = current sensing resistor, A = differential amplifier, LOAD = programmable constant current active load, MICRO = microcontroller, CHARGER = CC–CV charger.

During discharge time precisely controlled by a microcontroller (MICRO), the positive path of two 18650 Li-Ion batteries (BAT1, BAT2) are switched alternately by T1 and T2

power MOSFETs in a turn OFF before turn ON sequence (Figure 2). T1 and T2 are controlled via current drivers (DRV1, DRV2) by two digital outputs of MICRO. The sourced current during discharge pulses is sensed on a 0.01 Ohm resistor, (R) and is converted to compatible voltage by one high gain (a = 100) difference amplifier (A). A detailed electronic schematic of SWD device is presented in Figure A1 and SWD operating modes in Table A1 (Appendix A).

Battery parameters (U1, I1 and U2, I2) are measured during discharging pulses, with microcontroller's 10-bit ADC and programmable sampling rate. Sampled data are packed in the microcontroller's memory and sent together with battery temperature measurements, each minute via USB to the terminal software (Tera Term Pro v2.3) installed on the computer. The current flowing to the active load is fully programmable through the microcontroller internal DAC via the analog output signal (DSCH). After a complete discharge cycle, a charging cycle consisting of CC-CV can be performed with the CHARGER circuitry. During charging, there is no current flow through the active load. Continuous discharge of any battery combination or pulsed/switched discharge with dead time between pulses can be performed on the SWD device. Alternate usage of the internal electronic load or of an external load is possible via X1 connector.

Three sets of two NCR18650B cells with 3.2 Ah, (Panasonic, Osaka, Japan) [19] were selected for the pulsed discharge tests. Battery specifications are presented in Table 1.

Table 1. Panasonic NCR18650B specifications.

Rated Capacity at 25 deg. C	3200 mAh
Nominal Capacity at 25 deg. C	Min. 3250 mAh
	Typ. 3350 mAh
Nominal Voltage	3.6 V
Charging Method	CC-CV
Charging Voltage	4.2 V
Charging current	1625 mA
Charging Time	4 h
Cathode material	Nichel Oxide Based New Platform (NNP)

The programmed duty cycle (50%) has been determined by measurement, based on Equation (1):

$$\text{Duty\_cycle} = (p_w/T) \cdot 100\%, \tag{1}$$

where, p_w is the pulse width and T is the total period of the signal. The capacity of the battery is determined by:

$$C = I \cdot t \ [\text{Ah}], \tag{2}$$

where, I is the constant current and t is the time. The energy delivered during discharge (E_{tp}) has been calculated with Equation (4), while the total energy loss (E_{ts}) with Equation (3):

$$E_{ts} = E_{driver} + E_{switch} \ [\text{Wh}], \tag{3}$$

E_{driver} is the energy lost on the driver and E_{switch} is the energy consumed during switching time. If E_{driver} can be considered negligible, E_{switch} heavily depends on: discharge current rate, T1 and T2 drain-source voltage, T1 and T2 switching speed and load characteristic (resistive or inductive).

The remaining energy delivered by a battery in pulsed mode is:

$$E_{tp} = E - E_{ts} \ [\text{Wh}], \tag{4}$$

Batteries were marked as A1, A2; B1, B2; and C1, C2. Prior to perform each discharging cycles (more than 50 cycles), batteries were charged at full capacity (4.2 V, 3200 mAh) using the CC-CV method. Switched discharge method (50% duty-cycle) was programmed (Table 1). The complete discharge voltage threshold was set to 2.5 V in the firmware. The SWD has been connected to DC power and a USB cable was used for data transfer. The

switching time/duty-cycle was carefully verified using a Tektronix MSO41014 oscilloscope, prior of starting any data log.

2.4. Discharge Setups

Two types of discharge set-ups were investigated using our SWD and according to Figure 3 we have tested: (a) pulsed versus continuous discharge of a single cell and (b) switched with dead time versus parallel discharge using a set of two cells. The temperature sensors, model DS18B20 (Maxim Integrated/Analog Devices), has been attached to the casing of the batteries under the discharge using thermal grease for contact, while the ambient temperature in the lab has been set to 21 °C.

(**a**)   (**b**)
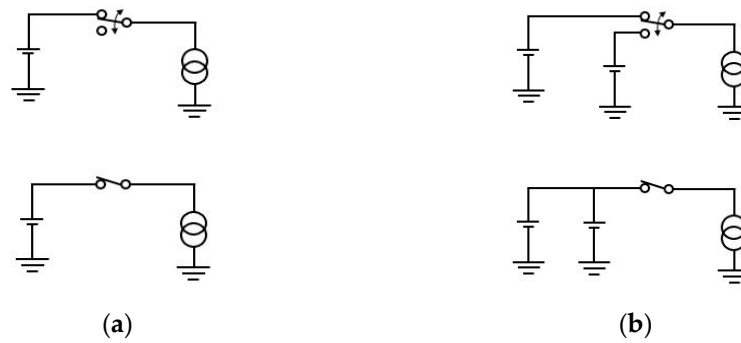
Figure 3. SWD discharge set-ups for: (**a**) one Li-Ion cell in pulsed and continuous mode (**b**) two Li-Ion cells in switched and parallel mode.

3. Results

3.1. SOC and Impedance Measurements Results

SOC values for cell A1 are given in Table 2 and the minimum impedance values are presented in Figure 4. The impedance values have raised by 2.81% between 10% SOC and 100% SOC. In order to relate pulsed discharge to SOC levels, voltage value at the end of each SOC discharge step has been noted in Table 2.

Table 2. SOC versus OCV and V_{SOCe}.

SOC [%]	0	10	20	30	40	50	60	70	80	90	100
OCV [V]	3.12	3.407	3.511	3.572	3.624	3.693	3.693	3.877	3.955	4.054	4.15
V_{SOCe}	2.52	2.84	3.05	3.14	3.22	3.29	3.36	3.44	3.52	3.61	4.15

Legend: SOC: state of charge, OCV: open continuous voltage, V_{SOCe}: voltage level at end SOC step.

(**a**)   (**b**)
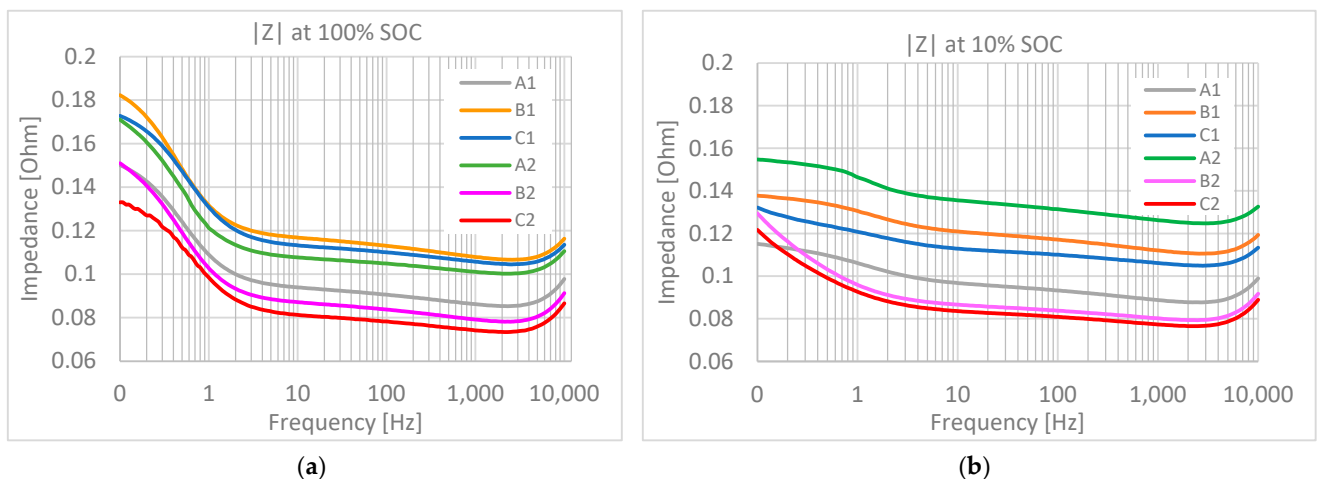
Figure 4. Impedance measurements: (**a**) at 100% SOC and (**b**) at 10% SOC.

EIS measurements taken on the VSP potentiostat have shown that the frequency corresponding to the minimum impedance of all tested 18650 Li-Ion cells is 2.3 kHz for both SOC states: 100% and 10%, respectively. Minimum impedance values differ for each battery, starting from 0.0734 Ω (C2) up to 0.106 Ω (A2) in 100% SOC state, and from 0.076 Ω (C2) up to 0.124 Ω (A2) in 10% SOC, as seen in Figure 4.

Impedance measurements taken at 10% SOC step clearly indicate that f_{Zmin} does not vary with SOC. According to [8], optimum pulsed discharge in terms of capacity took place at minimum impedance frequency; meanwhile, higher frequency values lead to an inferior response. In terms of practical applications (Figure 5), impedance variation in the 1 kHz–3 kHz range can be considered quasi-constant (0.004 Ω variation).
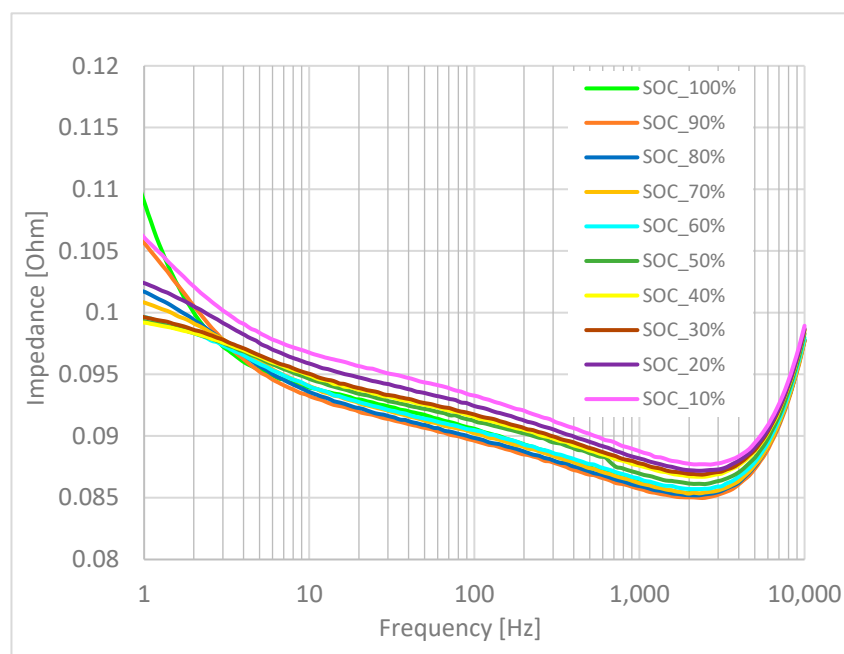
Figure 5. A1 cell impedance spectra for 10% step SOC values.

EIS analysis is used to evaluate the internal processes at the electrochemical interface layer of the battery. The Nyquist plot of cell A1 versus SOC is illustrated in Figure A2 (Appendix A). Using the circuit in Figure 1, the variation of the parameters corresponding to the high frequency spectrum with SOC is illustrated in Figure 6. The inductive behavior of a cell at high frequencies is associated with connectors and current collectors [15]. A Z-fit tool from Ec-lab had fitted the measured data with a 10^{-3} error. All parameters have shown SOC dependence. The ohmic resistance R1 (Figure 6a) and connectors resistance R2 (Figure 6b) are increasing towards the end of discharge, meanwhile the variation of inductance L2 shows a reduction with a fast decrease starting at 10% SOC. The increased values of the resistances towards the end of discharge are associated with the temperature rise within battery [17]. L2 decrease may be due to reduced electron flow that minimize the induced voltage effect. Based on the parameter's values, it can be stated that towards the low SOC interval, the impedance of the batteries becomes resistive.

3.2. Pulsed Discharge Mode

The SWD device showing a switching discharge session with two Li-Ion 18650 batteries and the associated temperature sensors is presented in Figure 7.

Figure 8 presents continuous and pulsed mode discharging curves of the batteries A1, B1 and C1 at 1C rate and various pulse frequencies (570 Hz up to 8.3 kHz, 50% duty-cycle). Time axis has been scaled for pulsed discharge data by duty-cycle factor reduction (0.5) since the discharge time for pulsed mode is double compared with continuous discharge

mode. The average discharge time of one 18650 Li-Ion cell down to 2.8 V in pulsed mode is 6 min to 8 min longer compared with continuous discharge as listed in Table 3. The corresponding capacity increase varies between 8.43% and 10.37% compared with continuous discharge capacity. An increased voltage reserve (cca.100 mV) over the entire discharge period appears on each battery and expands to 170 mV near the end of pulsed discharge cycle. The highest increase in discharge time was obtained at 5.8 kHz switching frequency. A similar result has been observed for A2, B2 and C2 cells with small variations caused by individual capacity variation. Increasing the switching frequency at 8.3 kHz (cell A1, Figure 8) does not improve the result. We did not find any correlation as reported by [8] between the f_{Zmin} (optimum frequency) requested to acquire the lowest cell impedance and our specific frequency (5.8 kHz) used for pulsed discharge.

(**a**)　　　　　　　　　　　　　　　　　　(**b**)
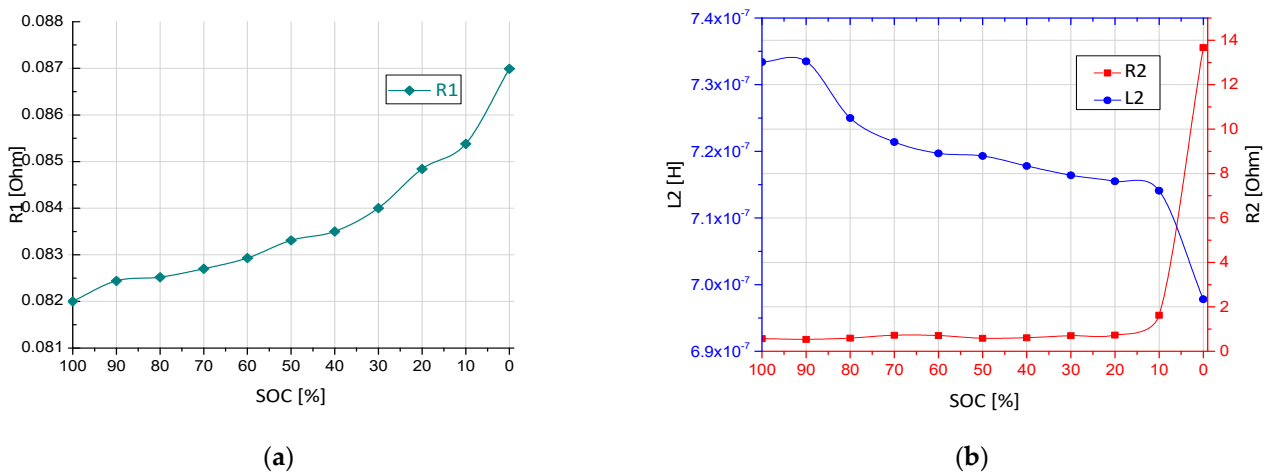
Figure 6. High frequency equivalent circuit parameters: (**a**) R1 parameter and (**b**) L2 and R2 parameters.
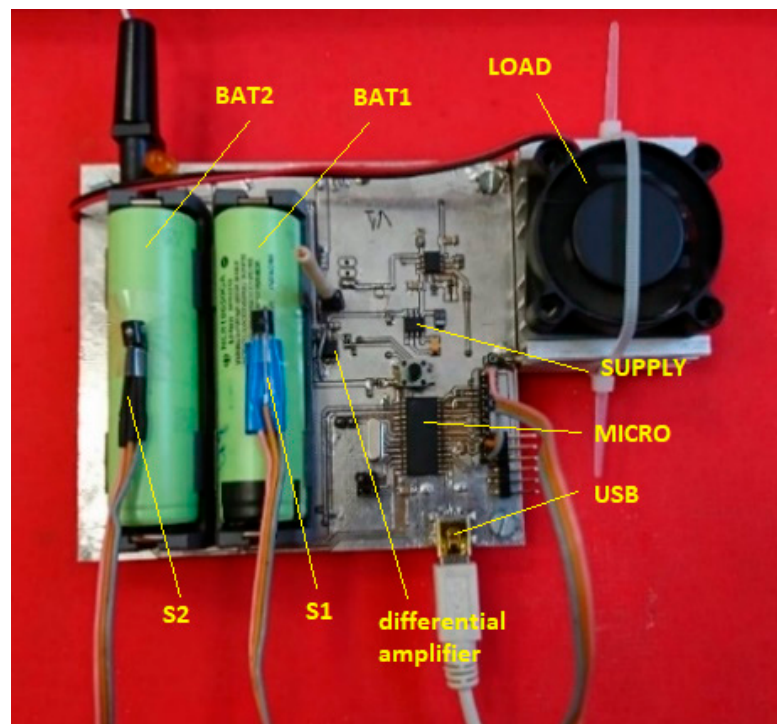
Figure 7. The SWD appearance during switched discharge.
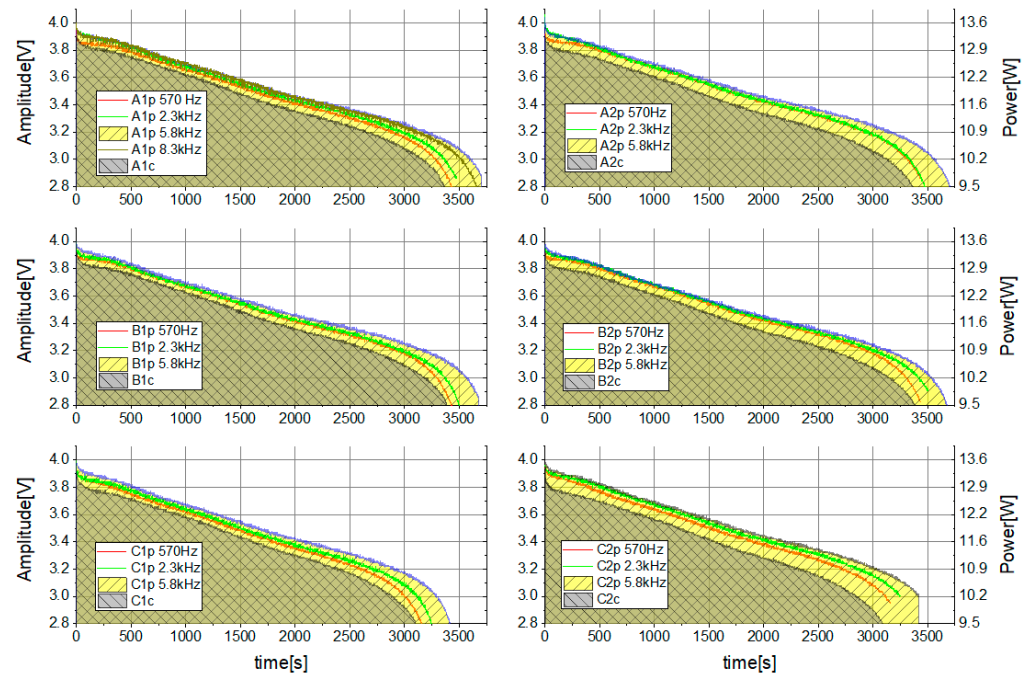
Figure 8. Cells A1A2, B1B2, C1C2 discharging curves; p-pulsed discharge mode, c-continuous discharge mode.

Table 3. Discharge data for one battery in pulsed versus continuous discharge.

Set-Ups	A1p versus A1c		B1p versus B1c		C1p versus C1c	
Capacity [Ah]	3.51	3.18	3.47	3.2	3.22	2.94
Capacity increase [%]	10.37		8.43		9.52	
Total discharge time	1 h:03 min	55 min	1 h:02 min	56 min	57 min	51 min
Surplus discharge time [min]	8		6		6	

Legend: p = pulsed discharge; c = continuous discharge; A1, B1, C1 = cells.

In this case, optimum frequency does not match the specific frequency found by us, which corresponds to a maximum energy released during pulsed discharge. The capacity in pulsed mode is up to 9.4% higher than capacity in continuous discharge when voltage cut-off limit is 2.8 V. For all six cells, the discharge power surplus obtained in pulsed mode compared with continuous mode is represented in Figure 9. There is a strong increase (near 1 W) at the end of discharge. At a discharge current of 1C, the power delivered by the cells varies between 13 W and 9.5 W. The power surplus extracted from the cells in pulsed mode with the described method and device varies in the range of 0.3 W to 1.2 W. An increase of 2.3% (near discharge start) up to 12.6% (near discharge end) of the delivered power without considering the switching losses discussed in Section 4.1, has been achieved. The total discharge energy delivered by A1 is 12.174 Wh. The surplus of energy resulted by using our proprietary SWD device, per an entire discharge cycle, is 1.42 Wh.

3.3. Switched Discharge Mode

As the specific frequency has been experimentally determined in the previous section, further analysis will relate only to the frequency of 5.8 kHz. The temperature has been measured at one minute acquisition rate during continuous, switched and parallel discharge modes. As expected, during the switched discharge at 1C/5.8 kHz and an ambient room temperature of 21 °C, the temperature of the batteries did not rise above 35 °C, Figure 10. The highest rise of the temperature, close to 40 °C, was measured during continuous discharge (T_A1c to T_C2c curves in). For all three sets of cells, the temperature curves for

switched discharge mode lay below the temperature of the parallel discharge, as seen in Figure 10.
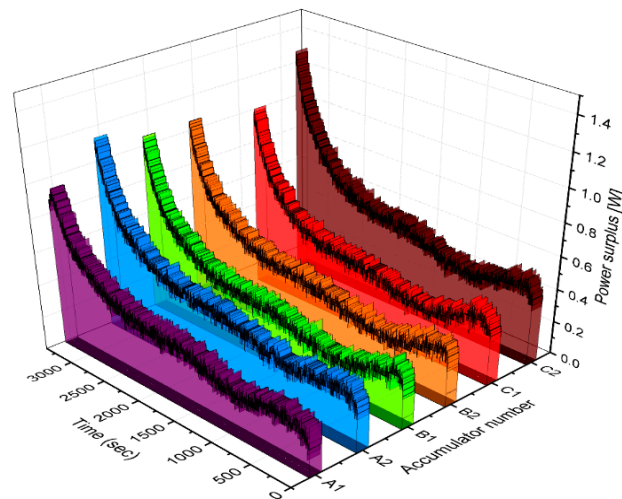
Figure 9. Power surplus: continuous delivered power subtracted from pulsed delivered power (5.8 kHz) at identical discharge rate (1C-rate).
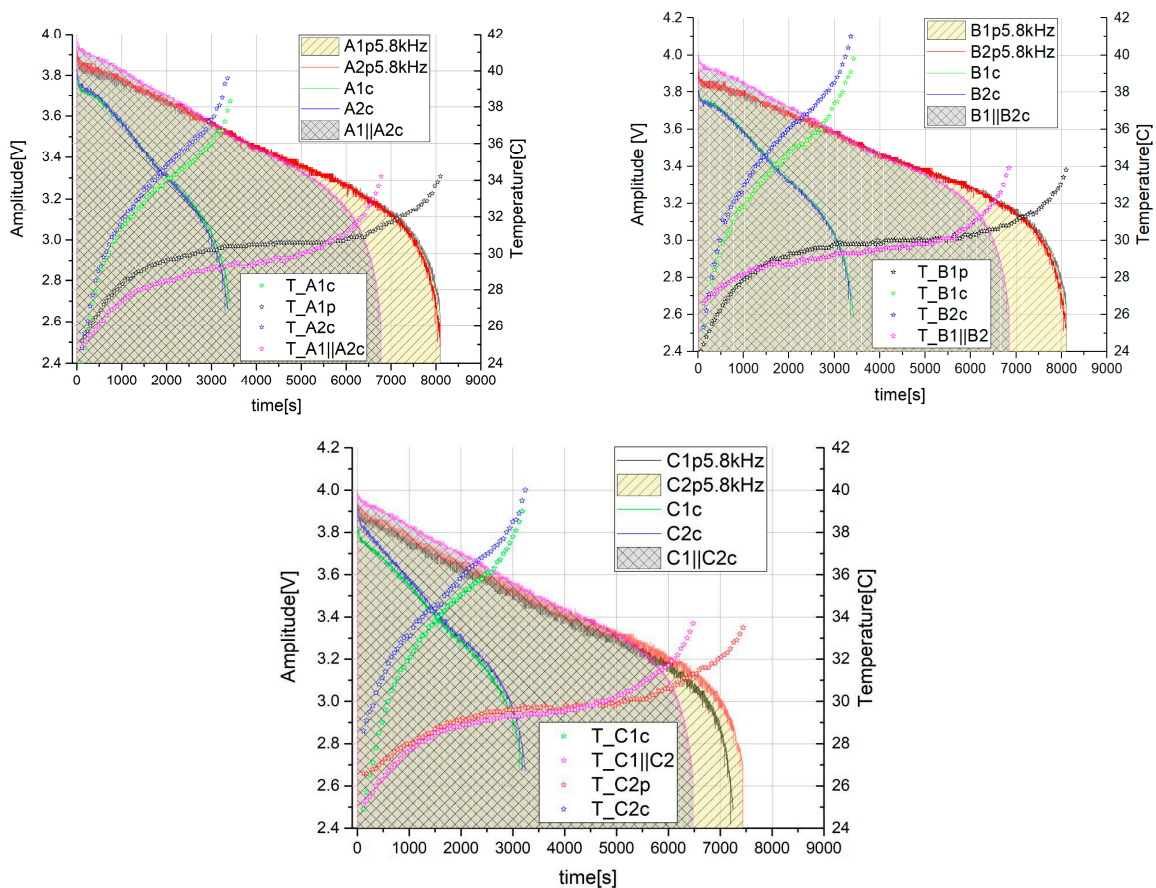
Figure 10. Temperature profiles and discharge curves profiles under continuous ("c"), switched ("p") and parallel discharge ("||c") batteries. T: temperature, A1, A2, B1, B2, C1, C2: cells.

A supplementary discharge time for energy extraction has been gained in switched mode compared with parallel mode, calculated to 2.8 V limit (Table 4). The extra discharge time varies from 15 to 21 min for all the repeated measurements. An increase in battery capacity in pulsed discharge mode of 11% to 16.6% is also visible.

Table 4. Discharge data for two switched batteries versus parallel connected.

Set-Ups	A1-A2p versus A1 ‖ A2c		B1-B2p versus B1 ‖ B2c		C1-C2p versus C1 ‖ C2c	
Capacity [Ah]	7.50	6.43	7.49	6.49	6.82	6.14
Capacity increase [%]	16.64		15.40		11.07	
Total discharge time	2 h:12 min	1 h:51 min	2 h:11 min	1 h:52 min	2 h:01 min	1 h:46 min
Surplus discharge time	21 min		19 min		15 min	

Legend: p = switched discharge, c = continuous discharge.

This extra discharge time translates in a supplementary energy of 12.66%, 12.1% and 8.29% (light yellow surface in Figure 10) for A1-A2, B1-B2 and C1-C2 set of batteries, respectively, in a single discharge cycle.

4. Discussion

4.1. Energy Loss during Switching

When two batteries are switched sequentially in order to provide continuous voltage to the load, any current flow directly from one battery to the other must be avoided in order to block parasitic cell charge and discharge respectively. This is possible through: (1) assuring a dead-band switching and mounting a capacitor for accumulation near the load (as we did in Figure A1 by C2 and C5), or (2) by mounting series low voltage drop diodes between the cells and the load [5]. Dead-band represents a short moment of time (2μs) when both switching MOSFETs are OFF. Method (1) is definitely better because it avoids supplementary power loss on diodes. Furthermore, a power loss on each MOSFET switching circuit emerges during discharge. This situation cannot be detoured. The real energy loss during switching (E_{switch}) has been captured by Tektronix MSO41014 oscilloscope (Figure 11) with C2 (Figure A1) completely removed. This removal during measurement is mandatory; otherwise, no dead-band waveform inspection is possible.
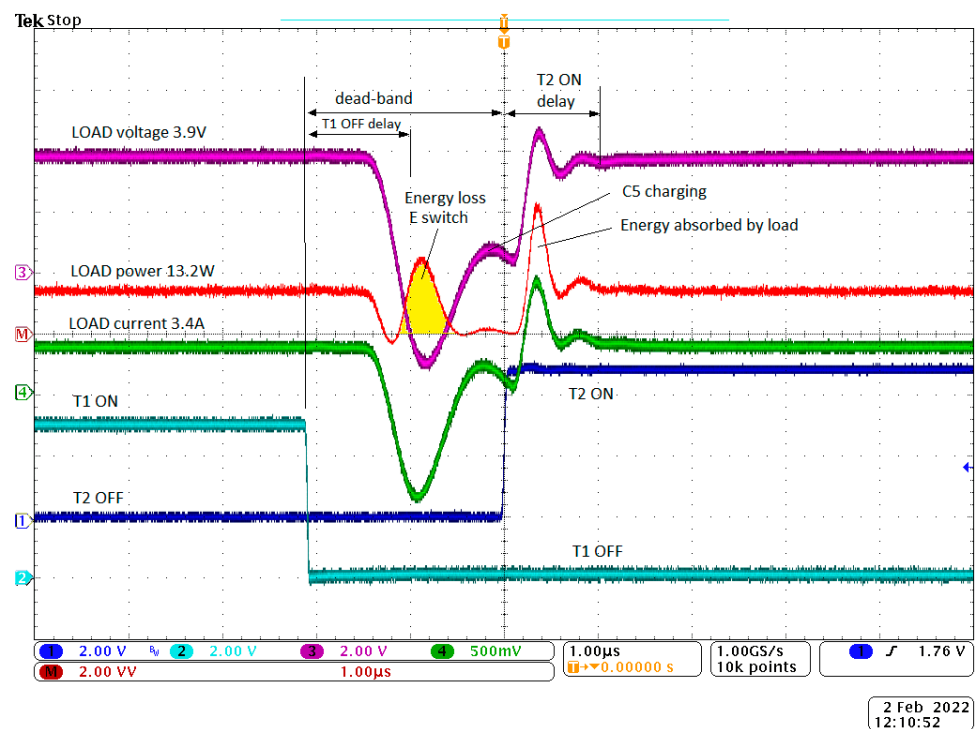
Figure 11. Measurement of the energy loss during switching. (Tektronix MSO4104 screen capture).

Table 5 lists the energy loss values over the entire discharge curve for the A1-cell. The switching number (n) represents how many switching occurs during the total discharge time (t).

Table 5. The energy loss during switching.

Nr.	Freq, F	Period, T	Total Discharge Time (t)	Switching Number $n = t/(T/2)$	Switch Loss (Sl) $n \cdot E_{switch}$	Continuous Loss (Cl) $t \cdot R_{DS} \cdot I^2$
	Hz	µs	s		W·h	W·h
1	570	1754	3435	3.915.621	0.006	0.034
2	2300	434	3476	16.081.433	0.024	0.0345
3	5800	172	3705	43.081.395	0.069	0.0358

Legend: Freq (F), period (T)—the switching parameters; (t)—the total discharge time; (n)—the numbers of switching during total discharge (t); (Sl)—energy lost during switching process on the MOSFET transistor; (Cl)—energy loss on the MOSFET internal drain-source during ON state; (R_{DS})—drain-source MOSFET resistance during conduction.

The switch loss is the energy lost on the switching transistor during total discharge time. Compared with the average value of the energy surplus obtained during the entire pulsed discharge cycle (Figure 9), the energy loss during switching (Sl) as well as the continuous energy loss (Cl) caused by the drain-source ON resistance (3.1 mΩ) of T1 and T2 (0.0358 W at 1C current rate), can be considered negligible.

4.2. Energy Surplus Delivery

It can be noticed (Figure 10, Table 4) that two parallel connected batteries provide superior energy until reaching 50% SOC (C battery) or 70% SOC (A, B cells). The same batteries, sequentially switched below discussed SOC, deliver higher energy than the parallel connected mode. This behavior was identical for all tested Li-Ion 18650 cells at various currents discharge rate and switching frequencies above the optimal frequency discharge. The result is better for batteries presenting higher initial capacity (A, B groups). Two batteries alternately switched at 1C and 50% duty-cycle have lower thermal dissipation than the same batteries discharged continuously at 1C. There were minor differences between battery temperature values caused by variations in the thermal contact between the flat sensor surface and curved battery, despite the use of thermal grease in the contact point. During switching, the rest period allows batteries to cool; they have better dissipation of the core temperature through the metallic case. Basically, the temperature measurement reveals the thermal stress produced during battery discharge, as the environmental temperature was constant.

In the Nyquist high frequency analysis, inductance L2 showed a descending trend; therefore, towards the end of the discharge, the voltage drop is mainly due to the resistive behavior of the cell. The relaxation periods in pulsed discharge combined with a reduced temperature growth applied to resistive impedance have led to an improved voltage characteristic below 50% SOC.

Table 4 shows the equivalent capacity of the batteries during switched discharge versus parallel continuous discharge considered as reference. The increase during switched discharge represents an amount of energy which does not dissipate to heat in the extraction process. The increase is visible, starting with the optimum frequency discharge corresponding to the lowest cell impedance, with a maximum increase at frequencies about 2.5 times higher. The optimum frequency corresponding to the minimum impedance is measured by the EIS technique, in which a small perturbation sinusoidal signal is applied to the battery, while the specific frequency was determined with SWD, by applying considerably higher rectangular current pulses that create strong perturbation until full discharge. Therefore, we can conclude that the specific frequency is dependent on perturbation magnitude, as well as on the external circuit which introduces parasitical inductances and capacitances. The design of the external PCB circuit must be carefully developed so that the losses are minimal. A possible resonance between the battery and its external switching electrical path may exist, but further investigations are necessary. In most off-grid power walls, the lowest discharge voltage level of the Li-Ion cells is limited down to 2.8 V to acquire a useable minimal voltage at the DC-AC inverters input. For example, seven Li-Ion series connected

(7 s) bank has a minimum threshold value of 7 × 2.8 V = 19.6 V. There is significant energy surplus extracted above 2.8 V during switched discharge versus continuous discharge (Figure 10) which can be future exploited in BMS driven Li-Ion banks.

5. Conclusions

In this paper, pulsed discharge of one Li-Ion 18650 cell and switched discharge of two Li-Ion pairs have been investigated. Three sets of two batteries and more than fifty measurements have been used to validate our results. Several conclusions can be drawn. Pulsed discharge of one Li-Ion 18650 cell and switched discharge of two Li-Ion 18650 cells on our proprietary device SWD have revealed that a specific frequency corresponding to a maximum output exists (5.8 kHz for Panasonic Li-Ion 18650) but there is no strict correlation with the optimum frequency described by literature corresponding to the lowest cell impedance due to the different perturbation level experienced by the battery. Values below and above 5.8 kHz resulted in a lower energy output, but still higher than continuous discharge. Further investigation is necessary for identifying the cause behind the specific frequency in pulsed discharge mode. The highest increase in power efficiency delivery has been found at medium and low SOC values. In this interval, the temperature measurement has indicated a reduction and the Nyquist analysis of the high frequency spectrum revealed a diminution of the inductance values. Pulsed discharge lasted 6 to 8 min longer, which implies a capacity up to 9.4% higher than the capacity in continuous discharge. In switched discharge the equivalent capacity increase was up to 16.6% higher compared with continuous discharge, and corresponded to an extra discharge time close to 20 min. This gain represents a significant quantity of energy supply that can be used on a load (a DC/AC inverter). Provided that the energy loss on the switching electronics proved to be insignificant, it can be concluded that the main reason of the total energy increase was the switching quality of the cells circuit and the existence of a proper dead-band during switching. Further work will determine the influence of switched discharge on the lifetime of a bank of accumulators (BMS included) and the variation of energy surplus with aging.

Author Contributions: Conceptualization, V.S.; methodology, V.S. and O.-R.B.; software, V.S.; validation, V.S. and O.-R.B.; formal analysis, O.-R.B.; investigation, V.S.; resources, O.-R.B.; data curation, O.-R.B.; writing—original draft preparation, O.-R.B. and V.S.; writing—review and editing, V.S and O.-R.B.; visualization, O.-R.B.; supervision, V.S.; project administration, V.S.; funding acquisition, V.S. and O.-R.B. All authors have read and agreed to the published version of the manuscript.

Funding: This research was founded from the MCID through the "Nucleu" Programe within the National Plan for Research, Development and Innovation 2022-2027, project PN 23 24 02 01.

Data Availability Statement: Not applicable.

Acknowledgments: We acknowledge financial support from the MCID through the "Nucleu" Programe within the National Plan for Research, Development and Innovation 2022–2027, project PN 23 24 02 01 Publication cost was covered by the Ministry of Research, Innovation and Digitalisation through Programme 1—Development of the National Research and Development System, Subprogramme 1.2—Institutional Performance—Funding Projects for Excellence in RDI, Contract No. 37PFE/30.12.2021. We express our gratitude to our colleague, professor dr. eng. Emanuel Puşchiţă for his valuable suggestions.

Conflicts of Interest: The authors declare no conflict of interest.

Appendix A. Detailed Electronics Schematic of SWD
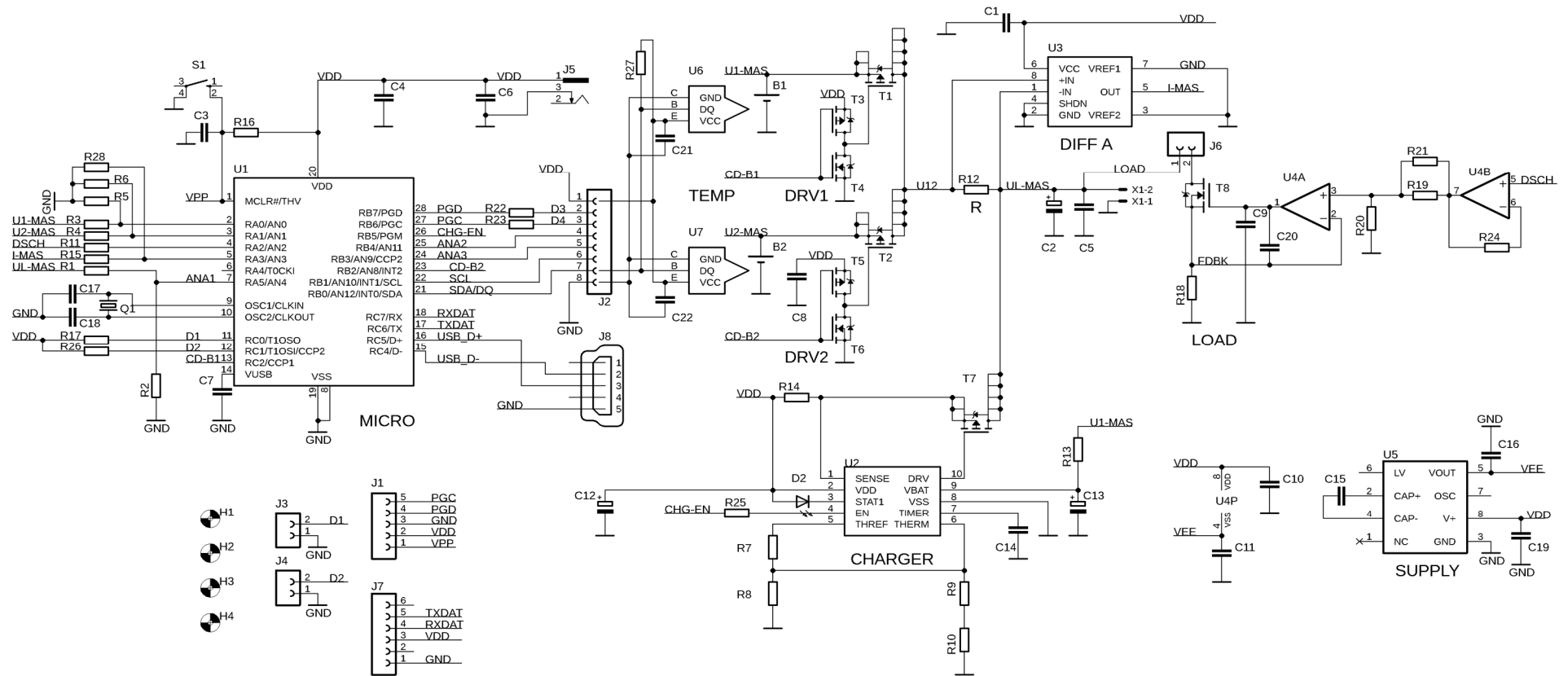
Figure A1. Detailed electronic schematic of SWD, the key elements: T1, T2, AP6681 U1 PIC18F25K50, U2 MCP73841, U3 TSC2012, U4 MCP6022, U5 ICL7660, U6, U7 DS18B20, T7 AP6681, T8 IRF2807 on heat sink and forced air cooled.

The device schematic and printed circuit board (PCB) has been generated using a free version of Eagle CAD. The PCB file was converted to be manufactured by a CNC Protomat S62 (LPKF Germany) machine from our prototyping laboratory. The SWD firmware evolved during various preliminary tests in many versions and has been generated by a free compiler (JAL v1.6.0). It has been uploaded in the microcontroller's flash memory using a PICKIT4 (USA) programmer controlled by MPLAB X IPE v5.50 (USA) software. The switching sequence of the power switches, T1 and T2, is described in Table A1 for all operating modes. Prior starting any discharge/charge cycle, three jumpers must be set.

Table A1. SWD device operating mode.

Nr.	Operating Mode	T1	T2	Jumper (Figure A1)
1	Charge	ON	ON	J3ON, J6OFF
2	Continuous discharge	ON	ON	J3OFF, J6ON
3	Pulsed/switched discharge; dead-time = 2 μS	OFF-ON-OFF	ON-OFF-ON	J3OFF, J4ON, J6ON

Appendix B. The Nyquist Plot of A1 versus SOC
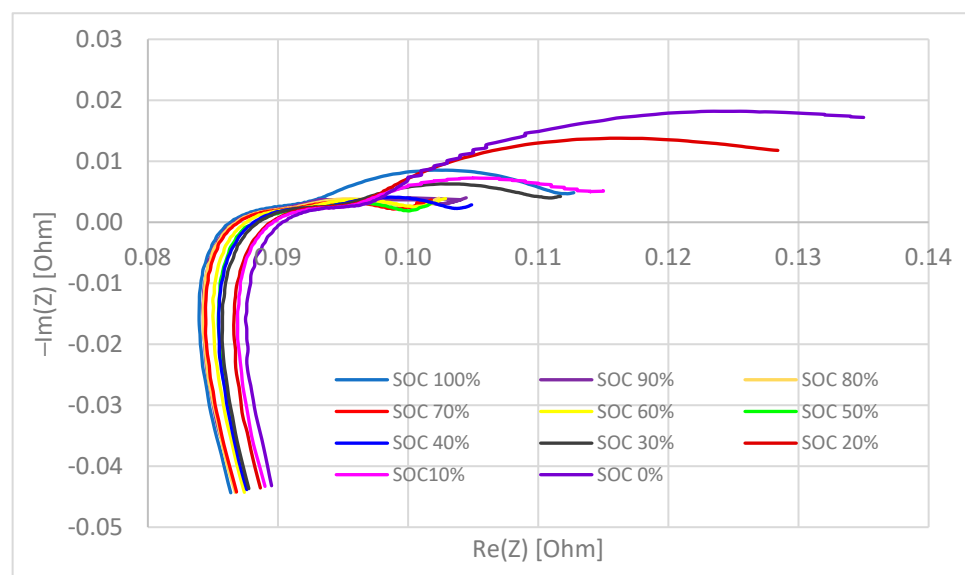
Figure A2. EIS spectrum for A1 cell.

References

1.　Keil, P.; Jossen, A. Aging of Lithium-Ion Batteries in Electric Vehicles: Impact of Regenerative Braking. *World Electr. Veh. J.* **2015**, *7*, 41–51. [CrossRef]
2.　Wikner, E. Lithium Ion Battery Aging: Battery Lifetime Testing and Physics-Based Modeling for Electric Vehicle Applications. Master's Thesis, Chalmers University of Technology, Gothenburg, Sweden, 2017.
3.　Jiang, J.; Zhang, C. *Fundamentals of Applications of Lithium-Ion Batteries in Electric Drive Vehicles*; John Wiley & Sons: Singapore, 2015; pp. 82–92.
4.　Huang, X.; Li, Y.; Acharya, A.B.; Sui, X.; Meng, J.; Teodorescu, R.; Stroe, D.-I. A Review of Pulsed Current Technique for Lithium-ion Batteries. *Energies* **2020**, *13*, 2458. [CrossRef]
5.　Benini, L.; Bruni, D.; Mach, A.; Macii, E.; Poncino, M. Discharge current steering for battery lifetime optimization. *IEEE Trans. Comput.* **2003**, *522*, 985–995. [CrossRef]
6.　DuBeshter, T.; Jorne, J. Pulse Polarization for Li-Ion Battery under Constant State of Charge: Part I. Pulse Discharge Experiments. *J. Electrochem. Soc.* **2017**, *164*, E3539. [CrossRef]
7.　Qin, Y.; Chen, X.; Tomaszewska, A.; Chen, H.; Wei, Y.; Zhu, H.; Li, Y.; Cui, Z.; Huang, J.; Du, J.; et al. Lithium-ion batteries under pulsed current operation to stabilize future grids. *Cell Rep. Phys. Sci.* **2022**, *3*, 100708. [CrossRef]
8.　Chen, L.-R.; Chen, J.-J.; Ho, C.-M.; Wu, S.-L.; Shieh, D.-T. Improvement of Li-ion Battery Discharging Performance by Pulse and Sinusoidal Current Strategies. *IEEE Trans. Ind. Electron.* **2013**, *60*, 5620–5628. [CrossRef]

9. Deng, Z.; Yang, L.; Cai, Y.; Deng, H. Maximum available capacity and energy estimation based on support vector machine regression for Lithium-ion battery. *Energy Proc.* **2017**, *107*, 68–75. [CrossRef]

10. Zheng, L.; Zhu, J.; Wang, G.; He, T.; Wei, Y. Novel methods for estimating lithium-ion battery state of energy and maximum available energy. *Appl. Energy* **2016**, *178*, 1–8. [CrossRef]

11. Sanchez-Gonzalez, A.; Medrano, N.; Calvo, B.; Martinez, P.A. A Multichannel FRA-Based Impedance Spectrometry Analyzer Based on a Low-Cost Multicore Microcontroller. *Electronics* **2018**, *8*, 38. [CrossRef]

12. Dong, T.K.; Kirchev, A.; Mattera, F.; Koval, K.; Bultel, Y. Dynamic modelling of Li-Ion Batteries Using an Equivalent Electrical Circuit. *J. Electrochm. Soc.* **2011**, *3*, 158. [CrossRef]

13. Leksono, E.; Haq, I.N.; Iqbal, M.; Soelami, F.X.; Merthayasa, U.G.N. State of Charge (SoC) estimation on LiFePO4 battery module using Coulomb counting methods with modified Peukert. In Proceedings of the 2013 Joint International Conference on Rural Information & Communication Technology and Electric-Vehicle Technology, Bandung-Bali, Indonesia, 26–28 November 2013. [CrossRef]

14. Concha, B.M.; Diard, J.P. *EIS Measurements: Potentio (PEIS) or Galvano (GEIS) Mode? That Is the Question*; EC-Lab Application Note #49; Bio-Logic Science Instruments: Seyssinet-Pariset, France, 2019.

15. Saidani, F.; Hutter, F.X.; Scurtu, R.-G.; Braunwarth, W.; Burghartz, J.N. Lithium-ion battery models: A comparative study and a model-based powerline communication. *Ad. Radio Sci.* **2017**, *15*, 83–91. [CrossRef]

16. Theiler, M.; Schneider, D.; Endisch, C. Experimental Investigation of State and Parameter Estimation within Reconfigurable Battery Systems. *Batteries* **2023**, *9*, 145. [CrossRef]

17. Morali, U.; Erol, S. Analysis of electrochemical impedance spectroscopy response for commercial lithium-ion batteries: Modeling of equivalent circuit elements. *Turk. J. Chem.* **2020**, *44*, 602–613. [CrossRef] [PubMed]

18. Landinger, T.F.; Schwarzberger, G.; Jossen, A. High frequency impedance characteristics of cylindrical lithium-ion cells: Physical-based modeling of cell state and cell design dependencies. *J. Power Sources* **2021**, *488*, 229463. [CrossRef]

19. Panasonic Energy, Product Specification. Rechargeable Lithium Ion Battery Model NCR18650B. 2017. Available online: https://www.imrbatteries.com/content/panasonic_ncr18650b-2.pdf (accessed on 11 November 2022).